# Electron interference in atomic ionization by two crossing polarized ultrashort pulses

J. M. Ngoko Djiokap,[1,*] A. V. Meremianin,[2] and N. L. Manakov[2]
[1]*Department of Physics and Astronomy, University of Nebraska, Lincoln, Nebraska 68588-0299, USA*
[2]*Department of Physics, Voronezh State University, Voronezh 394018, Russia*

(Received 2 December 2020; accepted 27 January 2021; published 10 February 2021)

Formation of geometrically regular interference patterns in the photoelectron momentum distributions (PMDs) corresponding to the photoionization of atoms by two single-color, *crossing* ultrashort pulses is investigated both analytically and numerically. It is shown that, in contrast to the photoionization by monochromatic pulses, PMDs for the ionization by crossing and co-propagating broadband pulses are essentially different (unless both pulses are linearly polarized), namely, when one pulse is linearly polarized along the propagation direction, $\hat{\mathbf{k}}$, of the circularly polarized (CP) pulse, then interference maxima (minima) of the ionization probability have the form of three-dimensional *single-arm* regular spirals which are wound along $\hat{\mathbf{k}}$. Next, the interference maxima (minima) of the ionization probability by a pair of crossing elliptically polarized pulses have the form of either Newton's rings or *two-arm* Fermat's spirals, depending on the position of a detection plane. Remarkably, these regular patterns occur only for certain values of the pulse ellipticities, and they become distorted for CP pulses. For both above-mentioned pulse configurations, the features of interference patterns depend on the time delay between pulses, their relative electric field amplitude, and relative carrier-envelope phase. Our predictions, illustrated by the numerical results for the ionization of H and He atoms by two orthogonal pulses, are quite general and we expect them to be valid for the ionization of any randomly oriented atomic or molecular target.

DOI: 10.1103/PhysRevA.103.023103

## I. INTRODUCTION

Recent advances in the experimental technique have made it possible to investigate the ionization of atoms and molecules by few-cycle electromagnetic pulses with tunable polarizations and carrier-envelope phases (CEPs) [1–6]. It was found that, for the time delay between ionizing pulses comparable with their duration, the photoelectron momentum distributions (PMDs) exhibit geometric patterns which bear a signature of the quantum interference of ionized electrons [1,2,7,8] similar to that observed by Ramsey [9]. In most experimental [1–3,6] and theoretical [7,8] works, only the ionization by linearly polarized (LP) pulses has been considered. In this case, the PMD exhibits a series of ring-shaped patterns superimposed by mutually perpendicular dark and bright dipole patterns [7].

The ionization of atoms by a pair of copropagating circularly polarized (CP) pulses has been investigated theoretically in Ref. [10]. In that work, based on the *ab initio* numerical solution of the time-dependent Schrödinger equation (TDSE) for the He atom and using perturbation theory (PT), it was shown that the PMD for the ionization by a pair of time-delayed CP pulses exhibits regular geometrical interference structures in the form of either Newton's rings (for corotating pulses) or two-arm Fermat's spirals (for counter-rotating pulses). An analysis of atomic ionization by both single-color and two-color time-delayed CP pulses was performed in Ref. [11], where it was demonstrated that the number of arms in spiral patterns depends on the number of photons required for single-electron ionization. These predictions have now been confirmed experimentally for multiphoton ionization of potassium atoms using single-color time-delayed CP femtosecond pulses [12,13] and of sodium atoms using bichromatic counter-rotating or corotating CP cycloidal femtosecond laser fields [14,15].

The prediction of Fermat's spirals in PMDs [10] has stimulated a number of theoretical works [16–29] which found the same spiral patterns in PMDs for other atomic [18–21,23–29] and molecular [16,17,22] photoionization processes with CP pulses taking place either in the multiphoton regime [16–19,22,25–29] or in the tunneling regime [20,21,23,29]. In Ref. [30], the semiclassical approach was used to analyze the interference patterns in PMDs. In all of these ionization processes, the two time-delayed CP pulses were always *copropagating* and the photoelectron has to be detected in the pulse polarization plane perpendicular to its propagation direction.

Recently, in Ref. [31] the time delay in the atomic ionization by a combination of LP and CP pulses was analyzed, including the case of perpendicularly propagating pulses. However, the authors of Ref. [31] did not report on the emergence of spiral interference patterns in PMDs.

So far, the emergence of spiral interference patterns in PMDs has been observed only for multiphoton ionization by femtosecond pulses with carrier frequencies in the optical region [12–14]. It is, however, of great interest to analyze the electron interference in the ionization by attosecond extreme ultraviolet (XUV) pulses, since the attosecond timescale is natural for the electron dynamics in an atom. Although the creation of isolated attosecond XUV pulses has been re-

*Corresponding author: marcelngoko@unl.edu

 

ported [4,32–34], the polarization of those pulses was linear. Recently, the polarization control of attosecond XUV pulses has been achieved [35]. Nevertheless, the production of attosecond XUV pulses with controllable polarization and time delay, which is necessary to observe the photoelectron interference with elliptically polarized (EP) pulses, remains a challenging task to date. In the present paper, we demonstrate that it is possible to avoid the use of counter-rotating copropagating pulses to observe the spiral patterns in PMDs, namely, the photoelectron interference can be, in principle, observed in the ionization by few-cycle *crossing*, rather than copropagating, isolated pulses, provided those pulses are phase-locked and the photoelectron detectors have sufficient angular resolution.

We investigate the PMD for the ionization of atoms by a pair of *crossing* few-cycle electromagnetic pulses using PT and illustrating PT predictions by the results of the direct numerical solution of the TDSE for the He atom. We demonstrate that PMDs corresponding to the ionization by copropagating and crossing few-cycle (i.e., broadband) pulses differ significantly when at least one of the pulses is polarized elliptically or circularly. For example, for copropagating CP and LP pulses neither ring-shaped nor spiral interference patterns can be seen in the PMD [10]. However, below (Sec. III A) we show that for perpendicularly propagating LP and CP pulses, the single-arm spiral patterns can be observed in PMD when (i) the polarization vector $\boldsymbol{\epsilon}_1$ of a LP pulse coincides with the propagation direction of a CP pulse and (ii) the photoelectron is emitted along the surface of any of the two cones whose axis is defined by the vector $\boldsymbol{\epsilon}_1$ and which are mirror images of each other with respect to the polarization plane of a CP pulse (see Fig. 1). For the ionization geometry shown in Fig. 1, interference fringes do not occur in PMD when the electron is detected in the polarization plane of a CP pulse. Note that no ring-shaped patterns (i.e., Newton's rings) can be observed in the PMD for the ionization by LP+CP pulses.

As is known [10,11,18,22], interference patterns in PMDs for copropagating CP pulses can be either Newton's rings (for corotating pulses) or two-arm Fermat's spirals (for counter-rotating pulses) but under no circumstances could they both emerge in the PMD for the same ionization process. We show (see Sec. III B), that for the ionization by orthogonal EP pulses, having some particular values of their ellipticities, two-arm Fermat's spiral patterns emerge in the PMD together with the Newton's rings in the same experimental setup. For example, when two ionizing pulses are identical and propagating perpendicularly, the Newton's rings can be seen in the PMD in a plane tilted at the angle $\pi/4$ with respect to the polarization plane of the second pulse ($xz$ plane in Fig. 2), while two-arm spiral patterns are seen in the PMD in a plane tilted at the angle $-\pi/4$ with respect to the $xz$ plane in Fig. 2. It is remarkable that the aforementioned interference patterns are geometrically regular when the sum of squared pulse ellipticities is equal to unity [see Eq. (35)] and they become distorted for purely CP polarized pulses. This is in contrast to the ionization by copropagating pulses when regular patterns occur for purely CP polarized pulses only [10]. For two identical orthogonal EP pulses, the regular interference patterns occur when pulse ellipticities are equal to $\pm 1/\sqrt{2}$, corresponding to a linear polarization degree of each pulse of $1/3$.

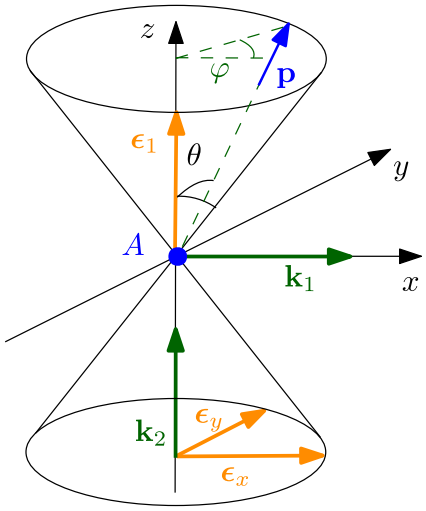


FIG. 1. Detection scheme for the observation of single-arm spiral patterns in PMD of atomic photoionization by perpendicular LP and CP pulses. The wave vector $\mathbf{k}_1$ defines the propagation direction of the LP pulse with the polarization vector $\boldsymbol{\epsilon}_1 \parallel \hat{\mathbf{z}}$, while $\mathbf{k}_2$ defines the direction of the right-hand CP pulse whose polarization ellipse is defined by the unit vectors $\boldsymbol{\epsilon}_x, \boldsymbol{\epsilon}_y$. The solid circle $A$ denotes an atomic target. Detected are the photoelectrons with momentum $\mathbf{p}$ emitted along the cone surface with the opening angle $\theta$. The PMD on the surface of the lower cone is a reflection of the PMD on the upper cone with respect to point $A$.

When ionizing EP pulses differ in intensity and CEP, the regular two-arm spiral and ring-shaped patterns can also be observed in the PMD for two detection planes tilted with respect to the polarization plane of a first (or second) pulse at the angles whose values depend on the pulse ellipticities and the relative electric field amplitude (Sec. III B). This PT prediction is confirmed numerically for the case of He atoms, where our numerical results for the triple-differential probability (TDP) are obtained by solving the full-dimensional TDSE. Note that below we have considered the ionization by *orthogonal* EP+EP pulses. However, it can be shown that our results remain qualitatively valid when the pulses cross at an arbitrary nonzero angle.

Although we have limited our consideration to the case of the first-order PT (i.e., single-photon) ionization process, the results of our treatment can be generalized to the case of multiphoton ionization. In the multiphoton regime, regular interference patterns in PMDs can be observed for the same detection geometries (see Figs. 1 and 2) as in the single-photon ionization with the only difference being the position and the number of spiral arms of the interference fringes.

This paper is organized as follows. In Sec. II, we present the PT parametrization of the ionization amplitude and discuss the differences between the ionization by monochromatic and short (i.e., broadband) pulses. In Sec. III, we analyze the probability of one-photon ionization of an atom by a pair of time-delayed orthogonal pulses. The ionization by orthogonal LP and CP pulses is considered in Sec. III A. The ionization by two orthogonal EP pulses is considered in Sec. III B. In Sec. IV, we discuss the possibility of experimental observations of the electron interference patterns for the proposed

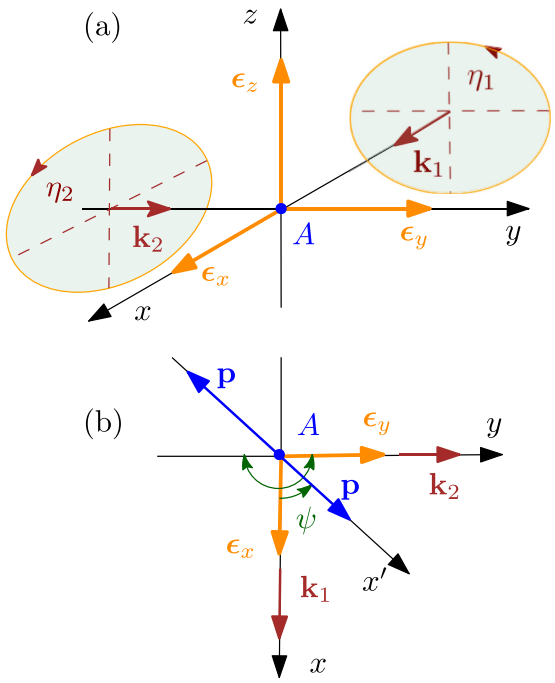


FIG. 2. (a) Geometry for the observation of two-arm spiral fringes for atomic photoionization by two short elliptically polarized pulses propagating in perpendicular directions. The wave vectors $\mathbf{k}_1$ and $\mathbf{k}_2$ define the directions of the laser beams. The unit vectors $\hat{\boldsymbol{\epsilon}}_y$, $\hat{\boldsymbol{\epsilon}}_z$ are directed along the major and minor axes of the polarization ellipse of the first pulse propagating along the $x$ axis. Similarly, the unit vectors $\hat{\boldsymbol{\epsilon}}_x$, $\hat{\boldsymbol{\epsilon}}_z$ define the polarization ellipse of the second pulse. Arrows on the polarization ellipses correspond to positive ellipticities, $\eta_1, \eta_2 > 0$. (b) Top view of the geometry on panel (a), including the detection plane. The $z$ axis is directed toward the reader, the detection ($zx'$) plane is tilted at the angle $\psi$ with respect to the ($zx$) plane, $-\pi/2 \leqslant \psi \leqslant \pi/2$. **p**'s show possible directions of the photoelectron momentum vector.

detection schemes. In Sec. V, we present a brief summary of the derived results. In Appendix A, we present the PT expressions for the dynamical parameters of the ionization amplitude for the H atom. Details of the procedure of the numerical solution of TDSE corresponding to the ionization of the He atom by a pair of orthogonal few-cycle pulses is described in Appendix B. Atomic units (a.u.) are used throughout the text unless otherwise specified.

## II. IONIZATION AMPLITUDE BY TWO SHORT PULSES WITHIN THE FIRST-ORDER PT

In the nonrelativistic limit and within the dipole approximation, the Hamiltonian of a quantum system (an atom or a molecule) subjected to an external electromagnetic field can be written as

$$\mathcal{H}(t) = H_0 - (\mathbf{D} \cdot \mathbf{F}(t)), \tag{1}$$

where $H_0$ is the Hamiltonian of an isolated system, $\mathbf{D}$ is the operator of the total dipole momentum, and $\mathbf{F}$ is the electric field strength.

For a monochromatic (i.e., sufficiently long) laser pulse, the electric field strength is given by

$$\mathbf{F}(t) = F\,\mathrm{Re}\,(\mathbf{e}\,e^{-i\omega t}), \tag{2}$$

where $\omega$ is the pulse frequency, $F$ is the electric field amplitude, and $\mathbf{e}$ is the electric field complex polarization vector normalized by $(\mathbf{e}^* \cdot \mathbf{e}) = 1$. Below we use the following parametrization for the polarization vector:

$$\mathbf{e} = (\hat{\boldsymbol{\epsilon}} + i\eta\hat{\boldsymbol{\zeta}})/\sqrt{1+\eta^2}, \tag{3}$$

where $\eta$ is the pulse ellipticity, $\hat{\boldsymbol{\epsilon}}$ and $\hat{\boldsymbol{\zeta}} = [\hat{\mathbf{k}} \times \hat{\boldsymbol{\epsilon}}]$ are the major and minor axes of the polarization ellipse. Here, $\eta > 0$ ($\eta < 0$) is for right (left) rotation of the electric field. Note that $\eta = +1$ for a right-hand circularly polarized (RCP) pulse, while $\eta = -1$ for a left-hand circularly polarized (LCP) pulse, and $\eta = 0$ for a LP pulse polarized along the $\hat{\boldsymbol{\epsilon}}$ axis. The circular and linear polarization degrees of laser pulses are denoted as $\xi$ and $\ell$, respectively, and they are defined by

$$\xi = \frac{2\eta}{1+\eta^2}, \quad \ell = \frac{1-\eta^2}{1+\eta^2}. \tag{4}$$

From these definitions, one can deduce the following auxiliary identities,

$$1+\ell = \frac{2}{1+\eta^2}, \quad 1-\ell = \frac{2\eta^2}{1+\eta^2}, \quad \eta^2 = \frac{1-\ell}{1+\ell}. \tag{5}$$

For a system subjected to a pair of long laser pulses, the electric field strength can be written in the form

$$\mathbf{F}(t) = \mathrm{Re}\,(\mathbf{e}_1 F_1 e^{-i\omega_1 t} + \mathbf{e}_2 F_2 e^{-i\omega_2 t}). \tag{6}$$

We suppose that the pulse intensity is not very large, so the first-order PT is applicable. Then, if $\omega_1 \neq \omega_2$, the energies of the ionized electrons will be either $E_b + \omega_1$ or $E_b + \omega_2$ ($E_b$ is the energy of an initial bound state) and their interference will be impossible. If $\omega \equiv \omega_1 = \omega_2$ and pulses are phase locked, then Eq. (6) can be rewritten as

$$\mathbf{F}(t) = F_1\,\mathrm{Re}\left(\tilde{\mathbf{e}}\,e^{-i\omega t}\right), \tag{7}$$

where $\tilde{\mathbf{e}} = (\mathbf{e}_1 + f\mathbf{e}_2)/\sqrt{1+f^2+2f\,\mathrm{Re}\,(\mathbf{e}_1^* \cdot \mathbf{e}_2)}$, $f = F_2/F_1$.

Comparing Eqs. (7) and (2), we conclude that the PMD in the ionization by two single-color long pulses is the same as PMD in the ionization by a single pulse with an effective polarization vector $\tilde{\mathbf{e}}$. More generally, we conclude that the angular structure of PMD remains the same no matter whether the system was ionized by copropagating or crossing single-color pulses.

The state of affairs changes drastically when the system is ionized by few-cycle pulses. Below we consider the situation when the system is ionized by two crossing ultrashort (i.e., broadband) pulses with polarization vectors $\mathbf{e}_1$ and $\mathbf{e}_2$. In this case, the electric field can be described by the formula

$$\begin{aligned}\mathbf{F}(t) = {} & F_1(t)\,\mathrm{Re}\,[\mathbf{e}_1 e^{-i(\omega t+\phi_1)}] \\ & + F_2(t-\tau)\,\mathrm{Re}\,[\mathbf{e}_2 e^{-i(\omega(t-\tau)+\phi_2)}],\end{aligned} \tag{8}$$

where $F_j(t)$ is the smooth envelope function, $\phi_j$ is the CEP of the $j$th pulse ($j = 1, 2$), and $\tau$ is the time delay between

pulses. For pulses having a $\cos^2$ envelope, the functions $F_j(t)$ can be written in the form

$$F_j(t) = [\theta(t + T_j/2) - \theta(t - T_j/2)]F_j \cos^2(\pi t/T_j), \quad (9)$$

where $\theta(t)$ is the Heaviside step function: $\theta(t < 0) = 0$ and $\theta(t \geqslant 0) = 1$, $T_j$ is the $j$th pulse duration, $T_j = 2\pi N_j/\omega$, with $N_j$ being the number of optical cycles corresponding to the carrier frequency $\omega$.

In the first-order PT, the transition amplitude of the single-electron ionization is defined by [36]

$$\mathcal{A} = i \int_{-\infty}^{\infty} \langle \mathbf{p}|\mathbf{D}\cdot\mathbf{F}(t)|i\rangle\, e^{i(E-E_b)t}\, dt, \quad (10)$$

where $|\mathbf{p}\rangle$ is the final continuum state of the electron having momentum $\mathbf{p}$ and $|i\rangle$ is the initial bound state of an atom.

Substituting Eq. (8) into Eq. (10), the integrals over time can be evaluated in a closed form. Among the ensuing terms, those containing complex conjugated vectors, $\mathbf{e}^*$, are small and are neglected in the below consideration [37]. Introducing the notation

$$J_j = F_j^{-1} \int_{-T_j/2}^{T_j/2} F_j(t)\, e^{i(E-E_b-\omega)t} dt, \quad j = 1, 2, \quad (11)$$

the amplitude Eq. (10) can be written in the form

$$\mathcal{A} = \frac{F_1}{2} e^{i(\pi/2-\phi)} \langle \mathbf{p}|\mathbf{D}\cdot\mathbf{e}_t|i\rangle, \quad (12)$$

where the effective polarization vector $\mathbf{e}_t$ is defined by

$$\mathbf{e}_t = J_1\mathbf{e}_1 + fJ_2\,\mathbf{e}_2\, e^{i\tau(E-E_b)+i\phi_{12}}, \quad (13)$$

where $\phi_{12} = \phi_1 - \phi_2$ is the relative CEP and $f = F_2/F_1$ is the relative field amplitude.

Assuming the initial atomic state as well as the residual ion state to be $S$ states, one can show that the matrix element of the dipole operator is proportional to the unit vector $\hat{\mathbf{p}} = \mathbf{p}/p$,

$$\langle f|\mathbf{D}|i\rangle = D_0(p)\hat{\mathbf{p}}, \quad (14)$$

where $D_0(p)$ is independent of the pulses polarization and the time delay $\tau$. As a result, the expression for the ionization amplitude becomes

$$\mathcal{A} = A_0(p)[J_1(\hat{\mathbf{p}}\cdot\mathbf{e}_1) + fJ_2(\hat{\mathbf{p}}\cdot\mathbf{e}_2)\, e^{i\Phi}], \quad (15)$$

where $\hat{\mathbf{p}} = \mathbf{p}/p$ is the unit vector along the photoelectron momentum $\mathbf{p}$, the dynamical amplitude parameter is defined by

$$A_0(p) = \frac{F_1}{2} D_0(p) e^{i(\pi/2-\phi_1)}, \quad (16)$$

and $\Phi$ is the Ramsey interference phase,

$$\Phi = (E + E_g)\tau + \phi_{12}, \quad (17)$$

where the photoelectron energy is $E = p^2/2$, the target binding energy $E_g = -E_b$ ($E_g > 0$), and $\tau$ is the time delay between the two pulses. Explicit expressions for the dynamical amplitude parameter $A_0 \equiv A_0(p)$ for the ionization of the ground state of the H atom are presented in Appendix A.

## III. AMPLITUDE AND TDP OF THE IONIZATION BY CROSSING SHORT PULSES

The expression for TDP of the ionization by a pair of arbitrarily polarized pulses can be obtained by taking the square modulus of the PT amplitude (15):

$$\mathcal{W} \equiv \frac{dW}{d\mathbf{p}} = |A_0|^2\big\{J_1^2|\hat{\mathbf{p}}\cdot\mathbf{e}_1|^2 + f^2J_2^2|\hat{\mathbf{p}}\cdot\mathbf{e}_2|^2 + 2fJ_1J_2\,\mathrm{Re}\,[(\hat{\mathbf{p}}\cdot\mathbf{e}_1^*)(\hat{\mathbf{p}}\cdot\mathbf{e}_2)\exp(i\Phi)]\big\}. \quad (18)$$

This parametrization of TDP is perfectly general and is valid for arbitrarily oriented pulses and electron escape directions. Moreover, one can show that Eq. (18) remains valid for a nonzero value of the angular momentum ($L_i \neq 0$) of an initial atomic state upon the addition of some isotropic (i.e., independent of the orientation of $\hat{\mathbf{p}}$) term $\propto (\mathbf{e}_t\cdot\mathbf{e}_t^*)$. Indeed, the above PT treatment [see Eqs. (10)–(13)] demonstrates that the parametrization of the photoionization amplitude for short pulses can be obtained from that for a single monochromatic pulse by applying the replacement $\mathbf{e} \to \mathbf{e}_t$. Thus, the parametrization of the TDP for an arbitrary initial bound state can be easily derived from the parametrization of the conventional photoionization cross section (see, e.g., Ref. [38]) by applying the above replacement. This procedure leads to the same parametrization (18) combined with the aforementioned isotropic term if $L_i \neq 0$. It means that the PT results formulated below are applicable to the ionization of any randomly oriented atomic or molecular target. However, in the case of the ionization of states with $L_i > 0$, the interference minima of TDPs will no longer be zeros due to the presence of an additional isotropic term.

The ionization by copropagating, time-delayed, CP pulses was analyzed in Refs. [10,11] where it was shown that PMDs registered in the polarization plane exhibit regular interference patterns being double-arm Fermat's spirals (for counter-rotating fields) or Newton's rings (for corotating fields).

Geometrically regular interference patterns do not occur in the ionization by copropagating pulses when both pulses are EP or when one pulse is polarized linearly and the second one is polarized circularly. On the contrary, as we shall see below, geometrically regular interference patterns do occur in the PMD for the ionization by a pair of *crossing* pulses, when both pulses are EP or for LP plus CP pulses. In the latter case, the *single-arm* Fermat's spirals can be observed in the PMD when pulses are propagating in perpendicular directions.

A careful analysis of parametrizations (15) and (18) leads to the conclusion that, for LP pulses, no new effects occur and PMDs for crossing and copropagating pulses have the same properties. Thus, below we limit our consideration to the two following cases: (i) one pulse is LP and the second one is polarized circularly and (ii) both crossing pulses are polarized elliptically.

### A. Ionization by crossing linearly and circularly polarized short pulses

Here, we study the PMD in the ionization by a pair of orthogonal pulses delayed in time by $\tau$, with one pulse being LP, $\eta_1 = 0$, and the other one being RCP or LCP, $\eta_2 = \xi = \pm 1$. In this case, the regular interference patterns emerge in the

PMD when the LP pulse is polarized along the propagation direction of the CP pulse, i.e., $\mathbf{e}_1 = \boldsymbol{\epsilon}_1 \parallel \hat{\mathbf{k}}_2$, see Fig. 1.

Analyzing the PT amplitude, Eq. (15), we shall deduce the pulse parameters and the detection geometry when the node lines of the ionization amplitude have the form of single-arm Fermat's spirals in the plane defined by the polar coordinates $(p, \varphi)$ of the momentum $\mathbf{p}$.

We assume the pulse envelopes to be identical, $J_1 = J_2$. For the sake of brevity, below we include the pulse envelope factor in the dynamic amplitude, $\mathcal{A}_0 = A_0 J_1$. By using the coordinate frame defined in Fig. 1, the photoionization amplitude (15) for the described pulse scheme takes the form

$$\mathcal{A} = \mathcal{A}_0[\hat{p}_z + g(\hat{p}_x + i\xi\hat{p}_y)\exp(i\Phi)], \tag{19}$$

where $g = f/\sqrt{2} = F_2/(\sqrt{2}F_1)$, with $F_1$ and $F_2$ being the electric field strengths of the LP and CP pulses, respectively. The connection of the Cartesian components $(\hat{p}_x, \hat{p}_y, \hat{p}_z)$ of the unit vector $\hat{\mathbf{p}} = \mathbf{p}/p$ with its spherical angles, $\theta, \varphi$, is given by

$$\begin{cases} \hat{p}_x = \sin\theta\cos\varphi \\ \hat{p}_y = \sin\theta\sin\varphi \\ \hat{p}_z = \cos\theta. \end{cases} \tag{20}$$

Inserting these identities into Eq. (19), we arrive at the following expression for the photoionization amplitude:

$$\mathcal{A} = \mathcal{A}_0\{\cos\theta + g\sin\theta\exp[i(\xi\varphi + \Phi)]\}. \tag{21}$$

Here, zeros of the expression in curly braces define the *kinematical* node lines of the ionization amplitude since they are independent of the atomic structure, while the zeros of the dynamical amplitude factor $\mathcal{A}_0$ define the *dynamical* nodes. One can show [39] that the dynamical nodes are absent in the ionization of the H atom in the dipole approximation (see Appendix A).

For $0 \leqslant \theta \leqslant \pi/2$, the kinematical node lines of the photoionization amplitude are defined by the equations

$$\cot\theta_0 = g = F_2/(\sqrt{2}F_1), \tag{22}$$

$$\varphi_{\text{nod}} + \xi\Phi = \pi \pm 2\pi n, \quad n = 0, 1, 2, \ldots. \tag{23}$$

Likewise, the kinematical node lines for $\pi/2 \leqslant \theta \leqslant \pi$ are defined by the equations

$$\cot\theta_0 = -g, \tag{24}$$

$$\varphi_{\text{nod}} + \xi\Phi = \pm 2\pi n, \quad n = 0, 1, 2, \ldots. \tag{25}$$

For $0 \leqslant \theta \leqslant \pi/2$, the interference maxima of $|\mathcal{A}|$ are defined by the condition (25) and $\tan\theta_m = g$; while for $\pi/2 \leqslant \theta \leqslant \pi$, interference maxima of $|\mathcal{A}|$ are defined by Eq. (23) and $\tan\theta_m = -g$. In both of those cases, one has that

$$\max|\mathcal{A}| = |\mathcal{A}_0|\sqrt{1+g^2} = \frac{|D_0(p)|}{2}\sqrt{F_1^2 + F_2^2/2}. \tag{26}$$

Note that nodes of the amplitude $\mathcal{A}$, as well as its interference maxima, are spirals in the three-dimensional momentum space. Those node lines are located on conical surfaces defined by the equations $\cot\theta_0 = \pm g$, while maxima lines are located on conical surfaces defined by the equations $\tan\theta_m = \pm g$.

Taking the square modulus of the photoionization amplitude (21), the TDP of the ionization by LP-CP orthogonal pulses evaluates to

$$\mathcal{W} = |\mathcal{A}_0|^2\sin^2\theta\{(g - \cot\theta)^2 + 4g\cot\theta\cos^2[(\Phi + \xi\varphi)/2]\}. \tag{27}$$

From this equation and Eq. (26), it follows that the interference maxima of TDP are

$$\mathcal{W}_{\max} = \frac{|D_0(p)|^2}{4}\left(F_1^2 + F_2^2/2\right). \tag{28}$$

As seen, photoelectron interference maxima are determined by a sum of pulse intensities rather than the squared sum of pulse amplitudes as in the case of the conventional interference of light waves.

If the photoelectron is detected in the polarization plane of the CP pulse (that plane is defined by $\theta = \pi/2$), then the TDP (27) reduces to $|g\mathcal{A}_0|^2$, which is a smooth function of $p$ and is $\tau$-independent. Thus, this situation is physically equivalent to the ionization by a single CP pulse. This PT prediction is also confirmed numerically by TDSE calculations for the He atom (not shown).

Let us analyze in more detail the PMD when the vector of the photoelectron momentum is directed along the surface of either of the two cones in Fig. 1. In this detection geometry, the polar angle $\theta$ is fixed and the TDP depends on the absolute value $p$ of the momentum vector $\mathbf{p}$ and its azimuthal angle $\varphi$, i.e., $\mathcal{W} = \mathcal{W}(p, \varphi)$. From Eq. (21), it follows that the amplitude $\mathcal{A}$ changes its sign under the replacement $(\theta, \varphi) \to (\pi - \theta, \pi + \varphi)$. It means that PMDs corresponding to the upper and lower cones in Fig. 1 are mirror images of each other. [More precisely, in this case one has $\mathcal{W}(\mathbf{p}) = \mathcal{W}(-\mathbf{p})$.] From Eqs. (17) and (27), it is seen that TDP is also invariant under the replacement $(\varphi, \phi_{12}) \to (\varphi + \varphi_0, \phi_{12} - \xi\varphi_0)$, where $\varphi_0$ is an arbitrary angle. Thus, by varying the relative CEP, $\phi_{12}$, one can rotate the PMD around the polarization direction of the LP pulse.

The TDP (27) comprises two terms, one of which, containing $\Lambda(f, \theta) = [g - \cot\theta]^2$, is independent of $\varphi$ and provides a constant background signal in the PMD registered on cone surfaces defined by the condition $\theta = \text{const}$. The second term in the TDP (27), containing $\Gamma(f, \theta) = 4g\cot\theta$, is similar to that for the case of the single-photon ionization of an $S$-state atom by a pair of time-delayed copropagating oppositely CP pulses [10]. The maxima and minima of this term have the form of three-dimensional Fermat spirals. Thus, for $\Lambda \gg |\Gamma|$, the visibility of spiral patterns in the PMD can be obscured by a strong constant background signal. On the contrary, for $\Lambda \ll |\Gamma|$, the second term in Eq. (27) dominates and spiral patterns will be clearly visible in the PMD. To analyze the $\theta$ dependence of both $\Lambda(f, \theta)$ and $\Gamma(f, \theta)$, in Fig. 4(a) we have presented the plots of $\Lambda$ and $\Gamma$ parameters for $f = 2$ and different $\theta$. The angles $\theta$, for which $\Gamma(f, \theta)$ is much greater than $\Lambda(f, \theta)$—favoring thus the spiral pattern occurrence – are clearly visible in Fig. 4(b), which is just a close-up of Fig. 4(a). For a fixed value of $\theta \neq \pi/2$ the visibility of spiral patterns driven by the second term in the TDP (27) can be controlled by tuning (increasing) the relative field amplitude parameter $f = F_2/F_1$. This can be achieved experimentally by

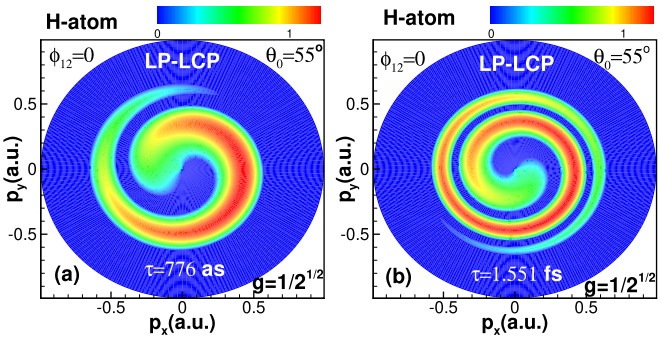


FIG. 3. TDP of the ionization of the H atom by a pair of orthogonal linear/left-circularly polarized (LP-LCP) pulses corresponding to the detection geometry defined in Fig. 1 for two different time delays in (a) and (b). The intensity of each pulse is $10^{14}$ W/cm$^2$. Pulses have identical envelopes, zero relative CEP, $\phi_{12} = 0$, and their duration is 1.551 fs, which is six optical cycles of the carrier frequency equal to 16 eV. The magnitudes of the TDP (in units of $10^{-2}$ a.u.) are indicated by the color scales in each panel.

decreasing the electric field strength $F_1$ of the LP pulse, noting that LP pulses are much easier to control experimentally than CP pulses.

To illustrate the above consideration, in Fig. 3 we present the PMDs for the ionization of the ground state of the H atom by LP+LCP perpendicularly propagating pulses calculated using first-order PT (see Appendix A) for two values of the pulse delay, $\tau = T/2$ in Fig. 3(a) and $\tau = T$ in Fig. 3(b), where $T = 1.551$ fs is the pulse duration. Both pulses have equal intensities, so the TDP has node lines for the opening angle $\theta = \theta_0 = 55^\circ$ [cf. Eq. (23)]. Also, the pulses have identical envelopes and zero relative CEP. As seen, the spiral is wound more densely for larger time delay. Note that for the ionization by LP+RCP pulses the spiral in the PMD changes its direction (not shown).

The predictions of the first-order PT agree well with the TDSE results for the He atom which are shown in Figs. 4(c)–4(f) for LP and CP pulses delayed in time by $\tau = T \approx 344$ as (where $T$ is the total pulse duration of each $\cos^2$ pulse) and having the relative amplitude $f = 2$. The corresponding opening angle in Figs. 4(c), 4(d) and 4(f) is $\theta_0 \approx 35^\circ$, while in Fig. 4(e) $\tilde{\theta}_0 = \pi - \theta_0 \approx 145^\circ$. The relative CEP $\phi_{12}$ between LP and CP pulses is fixed to zero in Figs. 4(c)–4(e), while $\phi_{12} = \pi$ in Fig. 4(f).

One sees that Fig. 4(c) for a right-handed ($\xi = +1$) CP pulse exhibits a counterclockwise single-arm spiral pattern, while Fig. 4(d) for a left-handed ($\xi = -1$) CP pulse exhibits a clockwise single-arm spiral pattern. Moreover, one sees that Fig. 4(e) for the lower cone with the opening angle $\tilde{\theta}_0 = \pi - \theta_0 \approx 145^\circ$ is a mirror of Fig. 4(c) for the upper cone with the opening angle $\theta_0 \approx 35^\circ$. It is also seen that the PMD in Fig. 4(f) for $\theta_0 \approx 35^\circ$ and $\phi_{12} = \pi$ coincides with that shown in Fig. 4(e) for $\tilde{\theta}_0 = \pi - \theta_0 \approx 145^\circ$ and $\phi_{12} = 0$, in full agreement with the above PT predictions.

Reducing the magnitude of the relative field amplitude parameter $f$ from 2 to 0.01, the same geometric patterns have been found (not shown) when detecting the photoelectron along the surface of a cone with an opening angle $\theta_0$ for $0.1 \leqslant f \leqslant 2$. Also, we observe that the magnitude of the TDP

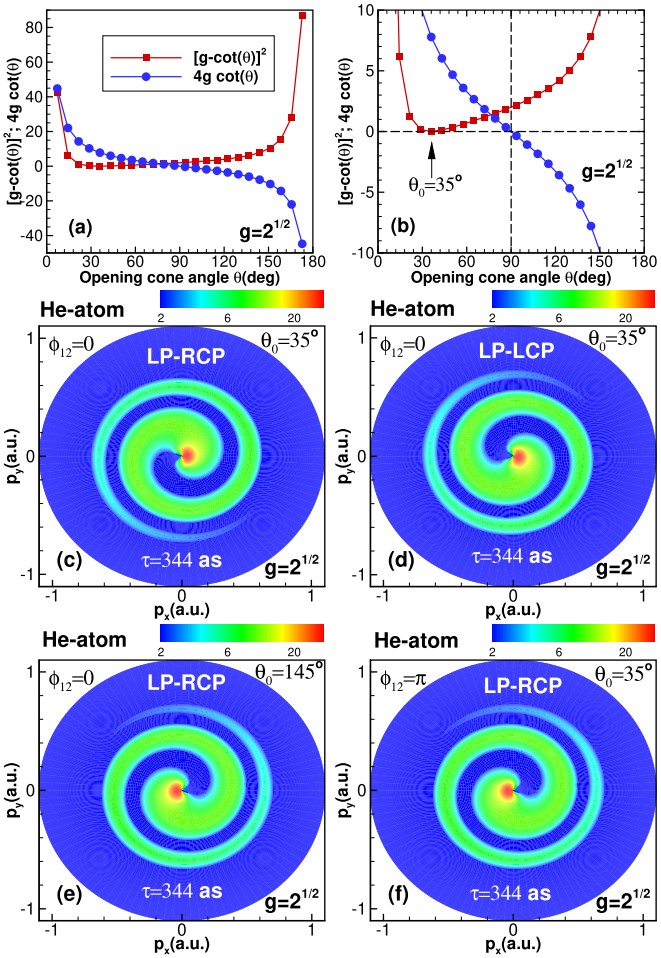


FIG. 4. Top row: Variation of the first term $[g - \cot\theta]^2$ and second term $4g\cot\theta$ in the TDP (27) with the opening cone angle $\theta$ for a fixed value of $g = f/\sqrt{2} = \sqrt{2}$, where $f = F_2/F_1$ is the ratio of the electric field strengths of the circularly polarized and linearly polarized pulses. Panel (b) is a close-up of panel (a), where the arrow therein indicates the value of the opening cone angle $\theta_0 \approx 35^\circ$ at which the first term of the TDP (27) vanishes, i.e., $\cot\theta_0 = g$. Middle row: TDSE results for the PMD, $\mathcal{W}$ [calculated using Eq. (B3)], recorded along the surface of a cone whose axis is defined by the propagation direction of the circularly polarized beam at the opening angle $\theta_0 \approx 35^\circ$. The counterclockwise or clockwise one-arm regular Fermat spiral pattern seen in (c) or (d) is produced by two orthogonal linear/right-circularly polarized (LP-RCP) pulses or by two orthogonal linear/left-circularly polarized (LP-LCP) pulses delayed in time by $\tau = T$. Here, each sine-squared pulse has a carrier frequency $\omega = 36$ eV, intensity $I = 10^{14}$ W/cm$^2$, total duration $T = 344$ as corresponding to three cycles. The relative CEP of the two pulses is $\phi_{12} = \phi_1 - \phi_2 = 0$. Bottom row: Panel (e) is the same result as in panel (c) but for the opening cone angle $\theta = \pi - \theta_0 \approx 145^\circ$. Panel (f) is the same result as in panel (c) but for the relative CEP $\phi_{12} = \pi$. In (c)–(f), the magnitudes of the TDP (in units of $10^{-3}$ a.u.) are indicated by the color scales.

decreases with $f$, which is also consistent with the PT result (28).

Note that the occurrence of single-arm spiral patterns in PMDs resulting from the ionization of atoms by two time-delayed short pulses was also predicted in Ref. [11]. However,

the single-arm spiral patterns discussed above and those considered in Ref. [11] have completely different origins, namely, in Ref. [11] the process of photoionization by time-delayed *two-color* copropagating CP attosecond pulses has been investigated. There, the occurrence of single-arm spiral patterns was predicted in the PMD registered in the polarization plane, which is in contrast to the present case where the interference effects are absent in the PMD registered in the polarization plane of the CP pulse. Here, we predict single-arm spiral patterns to be seen in the PMD when the electron is emitted along the surface of two detection cones whose axis is defined by the polarization direction of the LP pulse, which propagates perpendicularly to the CP pulse. Moreover, spiral interference fringes described in the present paper emerge in the *one-photon* process while the effect considered in Ref. [11] was caused by the interference of one- and two-photon ionization pathways.

### B. Ionization by two crossing elliptically polarized short pulses

Below we analyze the ionization geometry shown in Fig. 2(a), when an atom is ionized by two EP pulses delayed in time and coming from perpendicular directions. We choose the $x$ axis of the laboratory frame to be defined by the propagation direction of the first pulse, $\hat{\mathbf{k}}_1 \parallel \hat{\boldsymbol{\epsilon}}_x$, and the $y$ axis to coincide with the propagation direction of the second pulse, $\hat{\mathbf{k}}_2 \parallel \hat{\boldsymbol{\epsilon}}_y$. Thus, the $z$ axis is perpendicular to the propagation plane of the two pulses.

The complex polarization vectors of the two pulses are connected to the Cartesian basis vectors of laboratory frame as follows:

$$\mathbf{e}_1 = (\hat{\boldsymbol{\epsilon}}_y + i\eta_1\hat{\boldsymbol{\epsilon}}_z)/\sqrt{1+\eta_1^2}, \tag{29}$$

$$\mathbf{e}_2 = (\hat{\boldsymbol{\epsilon}}_x + i\eta_2\hat{\boldsymbol{\epsilon}}_z)/\sqrt{1+\eta_2^2}. \tag{30}$$

Assuming that both pulses have identical envelopes, $J_1 = J_2$, and using Eqs. (29) and (30), we can write the PT amplitude (15) as

$$\mathcal{A} = iA_0\left(\frac{\eta_1\hat{p}_z - i\hat{p}_y}{\sqrt{1+\eta_1^2}} + f\frac{\eta_2\hat{p}_z - i\hat{p}_x}{\sqrt{1+\eta_2^2}}\,e^{i\Phi}\right). \tag{31}$$

Denoting the spherical angles of the unit vector $\hat{\mathbf{p}}$ in the laboratory frame as $\theta$, $\psi$, the Cartesian coordinates of $\hat{\mathbf{p}}$ are expressed by

$$\begin{cases} \hat{p}_x = \sin\theta\cos\psi \\ \hat{p}_y = \sin\theta\sin\psi \\ \hat{p}_z = \cos\theta. \end{cases} \tag{32}$$

For further consideration, it is convenient to define the range of the angles to be, $0 \leqslant \theta \leqslant 2\pi$ and $-\pi/2 \leqslant \psi \leqslant \pi/2$. Inserting Eq. (32) into Eq. (31), we obtain

$$\mathcal{A} = iA_0\left(\frac{\eta_1\cos\theta - i\sin\theta\sin\psi}{\sqrt{1+\eta_1^2}} + f\frac{\eta_2\cos\theta - i\sin\theta\cos\psi}{\sqrt{1+\eta_2^2}}\,e^{i\Phi}\right). \tag{33}$$

Let us analyze the situation when the photoelectron is detected in a plane tilted at some angle $\psi$ with respect to the $xz$ plane in Fig. 2(b). Below we shall demonstrate how one can observe geometrically regular patterns in the PMD by tuning either the tilt angle $\psi$ or the relative field amplitude $f$. Such regular patterns are two-arm Fermat's spirals and Newton's rings, which are the same as in the ionization by copropagating CP pulses [10].

A careful inspection of Eq. (33) suggests that regular structures in the PMD occur when the following conditions are met:

$$\begin{aligned} \sin\psi &= \mu|\eta_1| = \mu\hat{\xi}_1\eta_1, \\ \cos\psi &= |\eta_2| = \hat{\xi}_2\eta_2, \end{aligned} \tag{34}$$

where $\hat{\xi}_j \equiv \operatorname{sign}\eta_j = \pm 1$ is the helicity of the $j$th pulse ($j = 1, 2$), and the parameter $\mu = \pm 1$ determines the tilt angle of the detection plane in Fig. 2, so $\psi = \arcsin|\eta_1|$ and $\psi = -\arcsin|\eta_1|$ for $\mu = 1$ and $\mu = -1$, respectively. Equations (34) demand that

$$\eta_1^2 + \eta_2^2 = 1, \tag{35}$$

which, according to Eq. (5), can be written in terms of the linear polarization degrees as $3\ell_1\ell_2 + \ell_1 + \ell_2 = 1$.

Assuming the conditions given by Eqs. (34) are met, after some simple transformations, Eq. (33) for the ionization amplitude becomes

$$\mathcal{A} = \frac{i\eta_1 A_0 e^{-i\mu\hat{\xi}_1\theta}}{\sqrt{1+\eta_1^2}}\{1 + \rho f e^{i[\Phi + (\mu\hat{\xi}_1 - \hat{\xi}_2)\theta]}\}, \tag{36}$$

where the real-valued parameter $\rho$ is given by

$$\rho = \frac{\eta_2}{\eta_1}\sqrt{\frac{1+\eta_1^2}{1+\eta_2^2}} = \frac{\hat{\xi}_2}{\eta_1}\sqrt{\frac{1-\eta_1^4}{2-\eta_1^2}} = \hat{\xi}_1\hat{\xi}_2\sqrt{\frac{1-\ell_2}{1-\ell_1}}. \tag{37}$$

Thus, the TDP, $\mathcal{W}_\psi(\rho) = \mathcal{W}$, of the photoionization by two orthogonal EP pulses whose ellipticities satisfy the conditions (35) can be written as [cf. Eqs. (5), (36)]

$$\mathcal{W}_\psi(\rho) = |\mathcal{A}|^2 = \frac{(1-\ell_1)}{2}|A_0|^2\{1 + \rho^2 f^2 + 2\rho f\cos[\Phi + (\mu\hat{\xi}_1 - \hat{\xi}_2)\theta]\}. \tag{38}$$

This equation is the key result of this section. It contains all the information about the positions of the geometrically regular interference patterns in the PMD as well as the magnitude of the corresponding TDP.

From Eq. (38), it is seen that the TDP has zeros only for $\rho f = \pm 1$ (i.e., for $\rho F_2 = \pm F_1$). Since $\rho$ is determined by the pulse's polarization [cf. Eq. (37)], one concludes that for pulses with the ellipticities satisfying the condition $\eta_1^2 + \eta_2^2 = 1$, one can always choose the relative field amplitude $f = F_2/F_1$ so the TDP will be zero when the phase of the cosine function in Eq. (38) is either $\pi + 2\pi n$ (for $\rho > 0$) or $2\pi n$ (for $\rho < 0$), where $n = 0, \pm 1, \pm 2, \ldots$. In the detection $zx'$ plane in Fig. 2, these conditions define either two-arm Fermat's spirals or Newton's rings, depending on the value of the parameter $(\mu\hat{\xi}_1 - \hat{\xi}_2)$. Accordingly, the tilt angle of the detection plane can take two values, $\psi = \mu\arcsin|\eta_1|$, $\mu = \pm 1$.

It is important to note that for a given value of the relative pulse intensity, $f$, the TDP has node lines only for some specific values of pulse ellipticities, $\eta_1$, $\eta_2$. As above, these node lines are either circles or two-arm spirals. Indeed, for a fixed $f$ we have $\rho = \pm 1/f$ and by solving the second equation in the chain (37) with respect to $\eta_1$ we obtain

$$\eta_1 = \pm\left(\frac{\rho^2 - \sqrt{\rho^2 + (\rho^2-1)^2}}{\rho^2-1}\right)^{1/2}, \tag{39}$$

$$\eta_2 = \pm\left(\frac{\sqrt{\rho^2 + (\rho^2-1)^2} - 1}{\rho^2-1}\right)^{1/2}, \tag{40}$$

where $\rho \neq 1$. For pulses with the same intensity, $f = 1$ and $\rho = \pm 1$. Accordingly, Eqs. (37) demand modules of the ellipticities to be equal: $|\eta_1| = |\eta_2| = 1/\sqrt{2}$, which means that $\eta_1, \eta_2 = \pm 1/\sqrt{2}$.

For the sake of clarity, below we consider separately the cases when (i) both pulses have the same helicities, $\hat{\xi}_1 = \hat{\xi}_2$, and (ii) the two pulses have opposite helicities, $\hat{\xi}_1 = -\hat{\xi}_2$. We illustrate the PT analysis by presenting PMDs obtained by the direct numerical solution of the TDSE for the He atom calculated for (i) with $f = 1$ and (ii) with $f = 0.5$. For case (ii), we also present the PMD for the H atom obtained by evaluating the first-order PT transition amplitude for $f = 1$.

#### *1. Ionization by two elliptically polarized pulses with the same helicity*

Below we consider the case when ellipticities of both pulses [cf. Eqs. (39), (40)] have the same sign:

$$\hat{\xi}_1 = \hat{\xi}_2. \tag{41}$$

According to Eq. (37), in this case $\rho > 0$ and it is more convenient to rewrite Eq. (38) as follows:

$$\mathcal{W}^{(+)}_{\psi}(\rho) = (1-\ell_1)|A_0|^2 \left\{ \frac{(1-\rho f)^2}{2} + 2\rho f \cos^2\left[\Phi/2 + \hat{\xi}_1(\mu-1)\theta/2\right] \right\}. \tag{42}$$

The interference minima of the TDP $\mathcal{W}^{(+)}_{\psi}$ are defined by

$$\Phi + \hat{\xi}_1(\mu-1)\theta_{\min} = \pi \pm 2\pi n, \quad n = 0, 1, 2, \ldots. \tag{43}$$

The magnitude of the TDP in these minima is

$$\mathcal{W}^{(+)}_{\min} = (1-\ell_1)\frac{(1-\rho f)^2}{2}|A_0|^2 = (1-\ell_1)\frac{(F_1 - \rho F_2)^2}{8}|D_0(p)|^2. \tag{44}$$

The interference maxima of the TDP in Eq. (42) are defined by

$$\Phi + \hat{\xi}_1(\mu-1)\theta_{\max} = \pm 2\pi n, \quad n = 0, 1, 2, \ldots, \tag{45}$$

while the magnitude of the TDP in these maxima is

$$\mathcal{W}^{(+)}_{\max} = (1-\ell_1)\frac{(1+\rho f)^2}{2}|A_0|^2 = (1-\ell_1)\frac{(F_1 + \rho F_2)^2}{8}|D_0(p)|^2. \tag{46}$$

From Eq. (44), it is seen that the interference minima of TDP become nodes when $\rho = 1/f = F_1/F_2$, where $\rho$ is given by Eq. (37). Let us consider this case in more detail. For $\rho = 1/f$, the TDP in Eq. (42) reduces to

$$\mathcal{W}^{(+)}_{\psi}(1/f) = 2(1-\ell_1)|A_0|^2 \cos^2[\Phi/2 + \hat{\xi}_1(\mu-1)\theta/2]. \tag{47}$$

For a positive detection angle, $\psi = \psi_0 > 0$, we have $\mu = 1$ and Eq. (47) becomes

$$\mathcal{W}^{(+)}_{\psi_0}(1/f) = 2(1-\ell_1)|A_0|^2 \cos^2(\Phi/2). \tag{48}$$

The corresponding PMD exhibits node lines and maxima lines in the form of Newton's rings. Indeed, node lines of the TDP are defined by the equation

$$\Phi = \pi \pm 2\pi n, \quad n = 0, 1, 2, \ldots, \tag{49}$$

while the interference maxima of the TDP in Eq. (48) correspond to the phase

$$\Phi = \pm 2\pi n, \quad n = 0, 1, 2, \ldots. \tag{50}$$

Both Eqs. (49) and (50) are equivalent to the condition $p =$ const, which defines Newton's rings in the PMD. The magnitude of the interference maxima of the TDP (48) is

$$\mathcal{W}^{(+)}_{\psi_0,\max}(1/f) = 2(1-\ell_1)|A_0|^2. \tag{51}$$

For $\psi = -\psi_0 < 0$, we have $\mu = -1$ and the TDP (47) reduces to

$$\mathcal{W}^{(+)}_{-\psi_0}(1/f) = 2(1-\ell_1)|A_0|^2 \cos^2\left(\Phi/2 - \hat{\xi}_1\theta\right). \tag{52}$$

Obviously, the node lines of $\mathcal{W}^{(+)}_{-\psi_0}$ correspond to the phase of the cosine satisfying the equations

$$\Phi - 2\hat{\xi}_1\theta_{\text{nod}} = \pi \pm 2\pi n, \quad n = 0, 1, 2, \ldots, \tag{53}$$

while the interference maxima of the TDP are defined by

$$\Phi - 2\hat{\xi}_1\theta_{\max} = \pm 2\pi n, \quad n = 0, 1, 2, \ldots. \tag{54}$$

Both above Eqs. (53) and (54) define Fermat spiral in the detection plane $(p_z, p_{x'})$ with the polar coordinates $(p, \theta)$. The solution of Eqs. (54) with respect to $\theta$ reads,

$$\theta_{\max}(p) = \hat{\xi}_1[(p^2/2 + E_b)\tau/2 + \phi_{12}/2 \pm \pi n]. \tag{55}$$

As seen, for $n$ and $n+1$, the values of $\theta$ differ in $\pi$, which means that the spiral has two arms. The direction of the spiral is determined by the sign of $\hat{\xi}_1$, namely, for $\hat{\xi}_1 = 1$ ($\hat{\xi}_1 = -1$) the spiral rotates counterclockwise (clockwise). The interference maxima of the TDP for $\psi < 0$ are the same as for $\psi > 0$, see Eq. (51). Comparing Eqs. (53) and (54), we conclude that the spirals representing node and maxima lines are mutually rotated by $\pi/2$.

When both pulses have the same intensity, we have $f = 1$ and $\rho = 1$ [as $\hat{\xi}_1 = \hat{\xi}_2$, cf. Eq. (37)], which means that $\eta_1 = \eta_2 = \pm 1/\sqrt{2}$. Consequently, the linear polarization degrees are $\ell_1 = \ell_2 = 1/3 \approx 0.33$ and the circular polarization degrees are $\xi_1 = \xi_2 = \pm(2/3)\sqrt{2} \approx \pm 0.94$ [cf. Eqs. (4)]. From Eqs. (34), we obtain that the tilt angle can take two values, $\psi = \pm\pi/4$, i.e., the detection planes are mutually orthogonal. We have used these pulse parameters to calculate PMDs for the ionization of the He atom by a pair of orthogonal EP pulses each having a sine-squared envelope profile, intensity of $I = 10^{14}$ W/cm$^2$, the total duration of $T \approx 344$ as, and

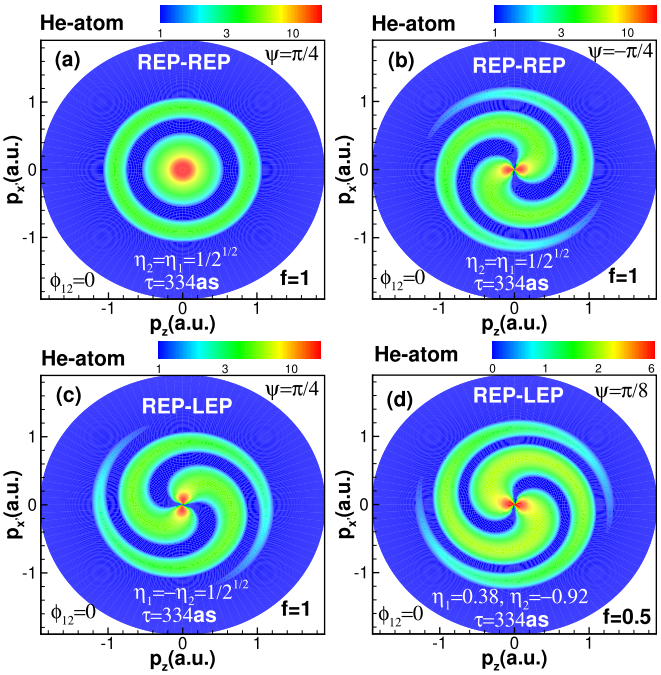


FIG. 5. The TDSE results for PMDs $\mathcal{W}_{\psi}^{(\pm)}(\rho)$ [calculated using Eq. (B3) for the He atom] in the detection plane $(p_{x'}, p_z)$. Shown in (a) is the TDP $\mathcal{W}_{\pi/4}^{(+)}(1)$ and in (b) is the TDP $\mathcal{W}_{-\pi/4}^{(+)}(1)$ of the photoionization produced by two time-delayed, orthogonal EP pulses with the same ellipticity $\eta_1 = \eta_2 = 1/\sqrt{2}$. Shown in (c) is the TDP $\mathcal{W}_{\pi/4}^{(-)}(-1)$ of the photoionization produced by two orthogonal EP pulses with opposite ellipticity: $\eta_1 = -\eta_2 = 1/\sqrt{2}$. In (a)–(c), $F_1 = F_2$ (i.e., $f = 1$). Panel (d) shows the TDP $\mathcal{W}_{\pi/8}^{(-)}(-2)$, corresponding to pulse ellipticities $\eta_1 = \sin\psi \approx 0.38$ and $\eta_2 = -\cos\psi \approx -0.92$, and the relative field amplitude $f \approx 0.5$. The magnitudes of the TDP (in units of $10^{-3}$ a.u.) are indicated by the color scales in each panel.

the zero relative CEP, $\phi_{12} = 0$. The time delay between the two pulses is $\tau = T$. The PMDs resulting from the numerical solution of TDSE for the He atom are shown in Figs. 5(a) and 5(b). Newton's rings are seen in the PMD in Fig. 5(a), which corresponds to $\psi = \pi/4$, while a counterclockwise two-arm spiral is visible in Fig. 5(b), which corresponds to $\psi = -\pi/4$. The observed features of PMDs are in full agreement with the above PT predictions.

### 2. *Ionization by two elliptically polarized pulses having opposite helicities*

Let us now consider the case when the two pulses have opposite helicities, $\hat{\xi}_1 = -\hat{\xi}_2$, which means that $\rho < 0$ [cf. Eq. (37)]. For $\rho < 0$, it is convenient to present the expression (38) for the TDP in the following form:

$$\mathcal{W}_{\psi}^{(-)}(\rho) = (1-\ell_1)|A_0|^2 \left\{ \frac{(1-|\rho| f)^2}{2} + 2|\rho| f \sin^2[\Phi/2 + \hat{\xi}_1(\mu+1)\theta/2] \right\}. \quad (56)$$

As seen, the spiral interference fringes in the PMD occur when $\mu = 1$. Remarkably, in this case the TDP $\mathcal{W}_{\psi}^{(-)}$ in Eq. (56) can be transformed into the TDP $\mathcal{W}_{-\psi}^{(+)}$ in Eq. (42) by making replacements $\theta \to \pi/2 - \theta$ and $\mu \to -\mu$. (The latter replacement implies that the tilt angle $\psi$ changes its sign, $\psi \to -\psi$.) In other words, the spiral PMD in the detection plane with the tilt angle $\psi$, corresponding to the co-rotating pulses, $\hat{\xi}_1 = \hat{\xi}_2$, transforms into the PMD in the detection plane with the tilt angle $-\psi$, corresponding to the counter-rotating pulses, $\hat{\xi}_1 = -\hat{\xi}_2$, by means of an overall rotation by the angle $\pi/2$ with subsequent reflection with respect to the axis $p_{x'}$.

For $\hat{\xi}_1 = -\hat{\xi}_2$ the TDP has node lines when $\rho = -1/f < 0$. In this case the expression (56) for the TDP simplifies to

$$\mathcal{W}_{\psi}^{(-)}(-1/f) = 2(1-\ell_1)|A_0|^2 \sin^2[\Phi/2 + \hat{\xi}_1(\mu+1)\theta/2]. \quad (57)$$

For $\psi = \psi_0 > 0$, according to Eqs. (34), we have $\mu = 1$, and Eq. (57) for the TDP evaluates to

$$\mathcal{W}_{\psi_0}^{(-)}(-1/f) = 2(1-\ell_1)|A_0|^2 \sin^2(\Phi/2 + \hat{\xi}_1\theta). \quad (58)$$

Node lines of the TDP (58) are defined by

$$\Phi + 2\hat{\xi}_1\theta_{\rm nod} = \pm 2\pi n, \quad n = 0, 1, 2, \ldots, \quad (59)$$

while the interference maxima of the TDP are defined by

$$\Phi + 2\hat{\xi}_1\theta_{\rm max} = \pi \pm 2\pi n, \quad n = 0, 1, 2, \ldots. \quad (60)$$

The magnitude of the interference maxima is the same as in Eq. (51).

For the tilt angle $\psi = -\pi/4$, from Eqs. (34) it follows that $\mu = -1$ and Eq. (56) for the TDP reduces to

$$\mathcal{W}_{-\psi_0}^{(-)}(-1/f) = 2(1-\ell_1)|A_0|^2 \sin^2(\Phi/2). \quad (61)$$

This equation means that Newton's rings emerge in the PMD. Comparing Eq. (61) with Eq. (48), one sees that positions of rings corresponding to nodes and maxima in those equations are reversed. Maxima in the TDP $\mathcal{W}_{\psi_0}^{(+)}$ are minima in the TDP $\mathcal{W}_{-\psi_0}^{(-)}$ and vice versa.

It is seen that the TDP $\mathcal{W}_{\psi_0}^{(-)}$, Eq. (58), differs from the TDP $\mathcal{W}_{-\psi_0}^{(+)}$, Eq. (52), by a phase of $\pi/2$ in the interference factor (i.e., the $\cos^2$-factor) and the sign at $\theta$. This is in accordance with the above remark [see the text below Eq. (56)]. Therefore, the PMD for pulses having opposite helicities, $\hat{\xi}_1 = -\hat{\xi}_2$, which corresponds to a detection plane with a tilt angle $\psi_0$, can be obtained from the PMD for pulses having equal helicities, which corresponds to a detection plane with a tilt angle $-\psi_0$ by means of an overall rotation by $\pi/2$ in the plane $(p_{x'}, p_z)$ and a reflection with respect to the axis $p_{x'}$.

In Fig. 5(c), we present numerical results for the ionization of the He atom by a pair of counter-rotating EP pulses having the same intensity, $f = 1$, and opposite ellipticities, $\eta_1 = -\eta_2 = 1/\sqrt{2}$. The PMD is shown for the tilt angle $\psi = \pi/4$. By comparing Figs. 5(c) and 5(b), one can observe the aforementioned symmetry property of the PMD. In Fig. 6, the PMDs for the ionization of the H atom are shown, obtained by calculating the first-order PT dipole matrix element (see Appendix A) for two values of the pulse delay $\tau$. Comparing Figs. 6(a) and 6(b) in which the time delay $\tau$ has doubled, one sees that the two-arm spiral in Fig. 6(a) becomes wound more densely, see Fig. 6(b). It is remarkable that Figs. 6(b) and 5(c) are quite similar despite the fact that they correspond to different atoms as well as pulse parameters (however, the

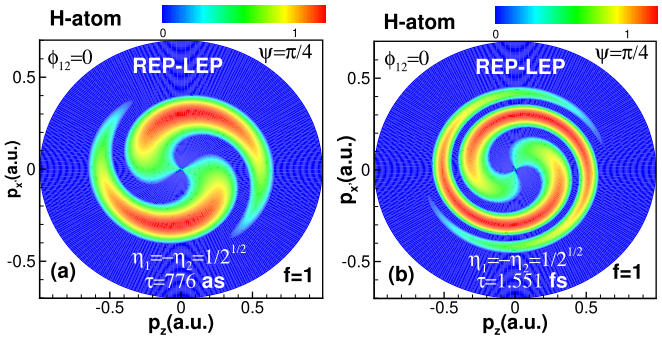


FIG. 6. TDP $\mathcal{W}^{(-)}_{\pi/4}(-1)$ of the ionization of the H atom by a pair of orthogonal EP pulses corresponding to the detection geometry in Fig. 2. Pulses are elliptically polarized with opposite ellipticities, $\eta_1 = -\eta_2 = 1/\sqrt{2}$. The intensity of each pulse is $10^{14}$ W/cm$^2$ ($f = 1$). Pulses have identical envelopes, their duration is 1.551 fs, which is six optical cycles of the carrier frequency equal to 16 eV. Panel (a) is for a time delay $\tau = T/2$, while panel (b) is for $\tau = T$. The magnitudes of the TDP (in units of $10^{-2}$ a.u.) are indicated by the color scales in each panel.

time delay in both cases is equal to the pulse duration). This observation elucidates the universal nature of the electron interference effects in the short-pulse ionization of atoms.

Let us also consider the ionization of the He atom by a pair of counter-rotating EP pulses with *unequal intensities* ($f \neq 1$), so the regular spiral interference patterns occur in the PMD for the detection plane tilted at an angle $\psi = \pi/8$ with respect to the polarization plane of the second pulse. For a given tilt angle $\psi = \pi/8$, the pulse ellipticities can be obtained from Eqs. (34), which give $\eta_1 = \sin(\pi/8) \approx 0.38$ and $\eta_2 = -\cos(\pi/8) \approx -0.92$. The corresponding circular polarization degrees of the two pulses are $\xi_1 \approx 0.66$ and $\xi_2 \approx 0.99$, while the linear polarization degrees are $\ell_1 = 0.75$ and $\ell_2 = 0.08$. As discussed above, the ionization amplitude and TDPs have node lines only for the relative field amplitude $f = \pm 1/\rho$ where the parameter $\rho$ is given by Eqs. (37). For the tilt angle of the detection plane $\psi = \pi/8$, we obtain $\rho \approx 1.9$, which means that electric field amplitude of the first pulse is roughly twice that of the second pulse, i.e., $f \approx 0.5$. The corresponding PMD obtained by solving the TDSE for the He atom is displayed in Fig. 5(d). As seen, the observed features of the *ab initio* calculated PMDs agree well with the PT predictions.

## IV. ON THE POSSIBILITIES OF THE EXPERIMENTAL OBSERVATION OF THE INTERFERENCE PATTERNS

For copropagating pulses, every atom in a reaction zone of an atomic cloud feels the same time delay between subsequent pulses. Therefore, ionization events registered by a photoelectron detector correspond to the same ionization process. This is generally not so when atoms are irradiated by crossing pulses. In this case, the time delay between pulses coming from different directions depends on the position of an atom in the reaction zone.

To clarify this issue, let us consider the situation when both pulses have plane wavefronts. Let $\mathbf{r}_j = (x_j, y_j, z_j)$ be the coordinates of a $j$th atom. The electric field at the point $\mathbf{r}_j$ is

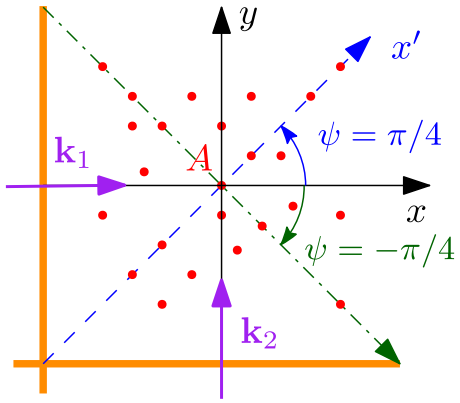


FIG. 7. Time delay for randomly placed atoms subjected to a pair of mutually perpendicular plane electromagnetic waves with wave vectors $\mathbf{k}_1$ and $\mathbf{k}_2$. Atoms are depicted as solid circles, thick solid lines denote wavefronts. Regular interference patterns occur in PMDs corresponding to detection planes depicted by dashed and dot-dashed lines. For every atom located in the $(zx')$ plane (the $z$ axis is directed towards the reader) defined by the tilt angle $\psi = \pi/4$ (i.e., the dashed line), the time delay is the same as for an atom located in a point $A$. For atoms located out of $(zx')$ plane, the time delay between pulses depends on coordinates $x$, $y$ of respective atoms.

(cf. Fig. 7)

$$\mathbf{F}(\mathbf{r}_j, t) = \mathrm{Re}\,\{\mathbf{F}_1(t - x_j/c)e^{-i\omega t + ik_1 x_j} + \mathbf{F}_2(t - y_j/c)e^{-i\omega t + ik_2 y_j}\}. \tag{62}$$

At this stage, we adjust the clock by replacing $t \to t + k_1 x_j/\omega = t + x_j/c$. As a result, the electric field becomes

$$\mathbf{F}(\mathbf{r}_j, t) = \mathrm{Re}\,\{\mathbf{F}_1(t)e^{-i\omega t} + \mathbf{F}_2(t - \tau_j)e^{-i\omega t + i\Delta\phi_j}\}, \tag{63}$$

where $\tau_j = (y_j - x_j)/c$ and $\Delta\phi_j = k_2 y_j - k_1 x_j$ is the phase shift between pulses caused by the difference between the paths traveled by those pulses, see Fig. 7. Since both pulses have the same carrier frequency, we have $k_1 = k_2 = 2\pi/\lambda$, where $\lambda = 2\pi c/\omega$ is the carrier wavelength. Therefore, $\Delta\phi_j = 2\pi(y_j - x_j)/\lambda$, and for the $j$th atom there occurs an additional time delay $2\pi(y_j - x_j)/(\lambda\omega) = (y_j - x_j)/c = \tau_j$ between pulses.

Note that for copropagating pulses, propagating along the $x$ axis, one has to replace $y_j \to x_j$, which means that $\tau_j = 0$ in this case, i.e., the time delay for all atoms in the reaction zone is the same.

Since photoelectron detectors have finite resolution, one has to integrate the TDP over the position of atoms located in the reaction zone. Let $l$ be the size of the reaction zone, then the time delay variation for atoms located at opposite edges of the reaction zone, $\Delta\tau$, has to be much smaller than the time delay between the pulses, $\Delta\tau \ll \tau$. This leads to the condition $l \ll \tau/c$. For $\tau \sim 10$ fs, we have $l \leqslant 1$ $\mu$m. This condition is achievable in current experiments [12]. For smaller pulse delays, the integration of TDP over time delays, corresponding to different atoms in the reaction zone, will spoil up interference effects since atoms in a gas phase are placed randomly.

However, if the detection plane is defined by a tilt angle $\psi = \pi/4$ (see Fig. 7), then for atoms in that plane $\Delta\phi_j = 0$

because $x_j = y_j$ there. This makes interference effects observable for such a detection scheme. Moreover, this feature of PMD can be used for measuring angles between the pulse beams, namely, by observing regular interference fringes in PMD for a specific value of the tilt angle $\psi_0$ between the detection plane and the polarization plane of the first pulse, one can conclude that the angle between the propagation directions of the two pulses is equal to $2\psi_0$.

Of course, wavefronts of real pulses are not ideal planes. Apart from that, the electric field strength varies in the cross section of the pulse beam. These circumstances make experimental observations of interference patterns a challenging problem. At the same time, the expected sensitivity of the interference patterns to various pulse parameters could make the experimental study of such interference phenomena useful for the purpose of the ultrashort pulse metrology.

## V. SUMMARY AND CONCLUSIONS

We have analyzed the momentum distributions of electrons emerging in the ionization of atomic targets by a pair of perpendicularly propagating, polarized, few-cycle electromagnetic pulses. We have shown that when both pulses strike an atom asynchronously (i.e., with a time delay), the PMD may exhibit geometrically regular interference patterns in the form of Newton's rings or Fermat's spirals, depending on the polarization state of each of the two pulses and the detection geometry. Although these interference patterns are similar to those emerging in the ionization of atoms and molecules by a pair of *copropagating* short CP pulses [10,11,22], we have found that the conditions for regular patterns to occur in PMDs are significantly different for collinear and crossing pulses. For example, no regular patterns could be observed in PMDs in the ionization by collinear LP and CP (or EP) pulses [10]. Further, no regular ring-shaped and spiral patterns could be observed simultaneously in the PMD for collinear pulses. Indeed, in the ionization by collinear CP pulses, the PMDs exhibit either ring-shaped patterns (for corotating CP pulses) or spiral patterns (for counter-rotating CP pulses) [10,11,22]. In the ionization by a pair of crossing EP pulses, both ring-shaped and spiral patterns can be observed in the same PMD (for certain electron emission planes), no matter whether the pulses had equal or opposite helicities (see Sec. III B).

We emphasize that the features of PMDs discussed above are not inherent to the ionization of either H or He atoms, and these atoms were considered merely as illustrative examples. Note also that our PT treatment of the ionization amplitude as well as the ionization probability was not specific to any particular target. Therefore, the predicted photoelectron interference effects could be observed in PMDs corresponding to photoionization of any randomly oriented target being that an atom, ion, or a molecule; the only limitations are the validity of the dipole approximation and not too large pulse intensities. The latter condition depends not only on peak pulse intensities but also on their carrier frequency [40]. For example, the ionization of Na atoms by femtosecond optical pulses with the intensity $\sim 10^{12}$ W/cm$^2$ occurs in the multiphoton regime [14], while the same intensity of XUV pulses in the ionization of inner shells means the applicability of the first-order PT [33]. The numerical simulations presented in Ref. [29] demonstrate that the interference patterns in PMDs wash out for the ionization of the Na atom by a pair of infrared pulses with intensities $\geqslant 10^{15}$ W/cm$^2$.

In the present paper, we have analyzed the ionization process within the first-order PT. Similarly to the case of the ionization by a pair of copropagating pulses [11], taking into account higher-order PT effects one can predict the emergence of multistart (three and more) spiral patterns in PMDs of the ionization by a pair of noncollinear pulses. Moreover, these modified spiral patterns would occur in PMDs for the same detection geometries as in the case of the first-order PT ionization process. A detailed analysis of the higher-order PT effects in the ionization by short crossing pulses will be the subject of a separate publication.

## ACKNOWLEDGMENTS

Research of J.M.N.D. is supported by the US Department of Energy (DOE), Office of Science, Basic Energy Sciences (BES), under Award No. DE-SC0021054; research of A.V.M. and N.L.M. is supported by the Ministry of Education and Science of the Russian Federation through Project No. FZGU-2020-0035. Computations were done using Crane of the Holland Computing Center at the University of Nebraska-Lincoln, and Stampede 2 at Texas Advanced Computing Center (TACC) under Grant No. TG-PHY120003.

## APPENDIX A: THE DYNAMICAL PARAMETER OF THE FIRST-ORDER PT IONIZATION AMPLITUDE FOR A HYDROGEN ATOM

For hydrogen, the matrix element of the electric dipole momentum vector between the initial $1S$ state and the final continuum state is proportional to the unit vector $\hat{\mathbf{p}} = \mathbf{p}/p$,

$$\langle f|\mathbf{d}|i\rangle = \langle \mathbf{p}|\mathbf{d}|10\rangle = D_0(p)\,\hat{\mathbf{p}}, \tag{A1}$$

where $|10\rangle$ is the initial $1S$ state of the H atom. An explicit expression for the parameter $D_0(p)$ can be derived by expanding the final state $|\mathbf{p}\rangle$ over the set of radial states $|pl\rangle$ having well-defined values of the orbital angular momentum quantum number $l$. For an initial $S$ state, only the final $P$ state $|p1\rangle$ ($l = 1$) contributes into $D_0$ due to the dipole selection rules. As a result, the parameter $D_0(p)$ can be expressed in terms of the radial matrix element,

$$D_0(p) = -\frac{e^{i\delta_1}}{\sqrt{4\pi}}\frac{\langle p1|r|10\rangle}{2p}, \tag{A2}$$

where $\delta_1$ is the Coulomb scattering phase, $\delta_1 = \arg\Gamma(1 - i/p)$ and the final state is normalized on the energy scale, $\langle p1|p'1\rangle = \delta(E - E')$, $E = p^2/2$. The radial matrix element in Eq. (A2) can be evaluated in closed form, which is

$$\langle p1|r|10\rangle = \frac{2^4 e^{-(2/p)\arctan p}}{(1+p^2)^{5/2}\sqrt{1-e^{-2\pi/p}}}. \tag{A3}$$

Noting the above, the first-order PT amplitude of the photoionization of the ground $1S$ state of an H atom by a single short pulse can be written in the form

$$\mathcal{A}_{1S} = A_0\,J(E)\,(\hat{\mathbf{p}}\cdot\mathbf{e}), \quad A_0 = \frac{F}{2}e^{i(\pi/2-\phi)}D_0(p), \tag{A4}$$

where

$$D_0(p) = -e^{i\delta_1} \frac{4\, e^{-(2/p)\arctan p}}{p(1+p^2)^{5/2}\sqrt{\pi(1-e^{-2\pi/p})}}. \tag{A5}$$

For a pulse envelope having $\cos^2$ shape and duration $T = 2\pi N/\omega$, where $N$ is the number of optical cycles of the carrier frequency $\omega$, $J(E)$ has the form

$$J(E) = \frac{\sin(T\epsilon/2)}{\epsilon(1-T^2\epsilon^2/4\pi^2)} = \frac{\sin(\pi N\epsilon/\omega)}{\epsilon(1-N^2\epsilon^2/\omega^2)}, \qquad \epsilon = E + E_g - \omega, \tag{A6}$$

where $E = p^2/2$ and $E_g = 1/2$ is the ionization potential of the H atom.

## APPENDIX B: PROCEDURE OF THE NUMERICAL SOLUTION OF THE TDSE FOR A HELIUM ATOM

Our numerical results for helium atoms are based on the *ab initio* solution of the two-electron TDSE in six dimensions for the atom exposed to two time-delayed, orthogonally propagating EP attosecond pulses. Details of our numerical procedures for time-delayed copropagating pulses can be found elsewhere [10,11,18,41]. Here, we extend our numerical methods to treat two orthogonal EP attosecond pulses. To solve the TDSE within the length gauge and the electric dipole approximation, we adopt the time-dependent close-coupling expansion [42,43] of the two-electron wave packet $\Psi(\mathbf{r}_1, \mathbf{r}_2, t)$ onto the orthonormal basis of bipolar spherical harmonics $\mathcal{Y}^{LM}_{l_1,l_2}(\hat{\mathbf{r}}_1, \hat{\mathbf{r}}_2)$,

$$\Psi(\mathbf{r}_1, \mathbf{r}_2, t) = \sum_L \sum_M \sum_{l_1,l_2} \frac{\Phi(r_1, r_2, t)}{r_1\, r_2} \mathcal{Y}^{LM}_{l_1,l_2}(\hat{\mathbf{r}}_1, \hat{\mathbf{r}}_2), \tag{B1}$$

where $L$ is the total angular momentum of the two-electron system, $M$ is its azimuthal quantum number, and $l_1, l_2$ are the individual electron angular momenta. To discretize $r_1$ and $r_2$ in the expansion coefficient $\Phi(r_1, r_2, t)$ of the wave packet $\Psi(\mathbf{r}_1, \mathbf{r}_2, t)$, we employ the fine-gridding scheme of the finite-element discrete variable representation (FEDVR) [44]. We use a two-dimensional grid ranging to 120 bohr radius, spanned by 60 finite elements (FEs) with an equal size of 2 bohr. An eight-point Gauss-Lobatto basis is used within each FE, which yields a total of 421 DVR functions spanning the 120 bohr radius.

To propagate $\Phi(r_1, r_2, t)$ in time in the presence of crossed EP pulses, we combine the real-space-product algorithm (a split-operator method) [45] together with Wigner rotation transformations at each time step from the atomic fixed frame in the laboratory coordinate system to the rotating frame defined by the external pulse polarization vector [46,47]. This procedure is quite accurate as long as the time step is sufficiently small, which we ensure in all our numerical TDSE calculations. The latter frame is rotated with respect to the laboratory frame by the Euler angles $(\alpha, \beta, \gamma)$ by using the Wigner rotation operator $D(\alpha, \beta, \gamma)$, whose matrix elements are

$$\langle L'M'|D(\alpha, \beta, \gamma)|LM\rangle = e^{iM'\alpha} d^L_{M',M}(-\beta) e^{iM\gamma} \delta_{LL'}, \tag{B2}$$

which is diagonal in $L$ but not in $M$. Thus the Wigner $d$-rotation function $d^L_{M',M}(\beta)$ is block diagonal within the $L$ representation. The Euler angle $\gamma$ defines a rotation around the atomic frame $z$ axis, $\beta$ defines a rotation about the rotating frame $y$ axis, and $\alpha$ defines a rotation about the rotating frame $z$ axis. Owing to the atomic spherical symmetry, the trivial rotation $\gamma$ can be set to zero. While an atom interacting with a LP field represents an axially symmetric problem, an atom interacting with an EP field does not. In the general case where $[H, L_z] \neq 0$, laser-atom couplings often introduce a mixing of different $M$'s across $L$'s, which tends to increase the complexity of the problem. This is the so-called $M$-mixing problem [46,47], which can be solved by computing, storing and applying very effectively from a numerical point of view the Wigner $d$-rotation function $d^L_{M',M}(\beta)$ in Eq. (B2).

For ionization of the He atom interacting with a LP pulse polarized along the $z$ axis (see, e.g., the first pulse in Fig. 1), one has $[H, L_z] = 0$ or $\alpha = \beta = 0$, so the magnetic quantum number $M$ is conserved. Parity is also a good quantum number. With the helium atom being initially in its $^1S^e$ ground state (where $M = 0$) and interacting with LP photons, $M$ is unchanged during the time propagation of the wave packet, thus reducing the numerical complexity of the problem.

In contrast, for EP pulses (see, e.g., the second pulse in Fig. 1 or the two pulses in Fig. 2), one has $[H, L_z] \neq 0$, so $M$ is not conserved. For the case of the second pulse in Fig. 1 where the circular polarization plane coincides with the $xy$ plane, one has $\beta = \pi/2$ and $\tan\alpha(t) = F_y(t)/F_x(t)$, with $F_x(t)$ and $F_y(t)$ being the $x$ and $y$ components of the electric field. For the case where the first EP pulse in Fig. 2 propagates along the $x$ axis, one has $\tan\beta(t) = F_y(t)/F_z(t)$ and $\alpha = \pi/2$. For the case where the second EP pulse in Fig. 2 propagates along the $y$ axis, one has $\tan\beta(t) = F_x(t)/F_z(t)$ and $\alpha = 0$.

At the end of the two pulses, i.e., at $t = T_f$, we calculate the TDP for single ionization of He to $He^+(1s)$ from the two-electron wave packet $\Psi(\mathbf{r}_1, \mathbf{r}_2, t)$ by projecting it onto correlated field-free Jacobi matrix wave functions $\Theta^{(-)}_{1s,\mathbf{p}}(\mathbf{r}_1, \mathbf{r}_2)$ [48]. For the energy range $0.1 \leqslant E \leqslant 30$ eV of the photoelectron considered here, we note that projecting onto uncorrelated field-free wave functions (a symmetrized product of Coulomb function and bound state) leads to the same TDP results, as discussed in Ref. [48]. The TDP, $\mathcal{W}$, for single electron ionization to the continuum with momentum $\mathbf{p} \equiv (p, \theta, \varphi)$ is thus

$$\mathcal{W} \equiv |\langle\Theta^{(-)}_{1s,\mathbf{p}}(\mathbf{r}_1, \mathbf{r}_2)|\Psi(\mathbf{r}_1, \mathbf{r}_2, T_f)\rangle|^2, \tag{B3}$$

where we include four total angular momenta ($L = 0 - 3$), their azimuthal quantum numbers $|M| \leqslant L$, all combinations of individual electron orbital angular momenta $l_1, l_2 = 0 - 5$, and their azimuthal quantum numbers $|m_1| \leqslant l_1$ and $|m_2| \leqslant l_2$.

[1] M. Wollenhaupt, A. Assion, D. Liese, C. Sarpe-Tudoran, T. Baumert, S. Zamith, M. A. Bouchene, B. Girard, A. Flettner, U. Weichmann, and G. Gerber, Interferences of Ultrashort Free Electron Wave Packets, Phys. Rev. Lett. **89**, 173001 (2002).

[2] F. Lindner, M. G. Schätzel, H. Walther, A. Baltuška, E. Goulielmakis, F. Krausz, D. B. Milošević, D. Bauer, W. Becker, and G. G. Paulus, Attosecond Double-Slit Experiment, Phys. Rev. Lett. **95**, 040401 (2005).

[3] T. Remetter, P. Johnsson, J. Mauritsson, K. Varjú, Y. Ni, F. Lépine, E. Gustafsson, M. Kling, J. Khan, R. López-Martens, K. J. Schafer, M. J. J. Vrakking, and A. L'Huillier, Attosecond electron wave packet interferometry, Nat. Phys. **2**, 323 (2006).

[4] A. Wituschek, L. Bruder, E. Allaria, U. Bangert, M. Binz, R. Borghes, C. Callegari, G. Cerullo, P. Cinquegrana, L. Giannessi, M. Danailov, A. Demidovich, M. D. Fraia, M. Drabbels, R. Feifel, T. Laarmann, R. Michiels, N. S. Mirian, M. Mudrich, I. Nikolov, F. H. O'Shea, G. Penco, P. Piseri, O. Plekan, K. C. Prince, A. Przystawik, P. R. Ribič, G. Sansone, P. Sigalotti, S. Spampinati, C. Spezzani, R. J. Squibb, S. Stranges, D. Uhl, and F. Stienkemeier, Tracking attosecond electronic coherences using phase-manipulated extreme ultraviolet pulses, Nat. Commun. **11**, 883 (2020).

[5] S.-Q. Zhang, Z.-J. Yang, Z.-X. Lei, W. Feng, S.-P. Zhou, K.-J. Yuan, X.-S. Liu, and J. Guo, Ultrafast photoionization of ions and molecules by intense orthogonally polarized laser pulses: Effects of the time delay, Chin. Phys. B **30**, 013201 (2021).

[6] Y. Mi, P. Peng, N. Camus, X. Sun, P. Fross, D. Martinez, Z. Dube, P. B. Corkum, D. M. Villeneuve, A. Staudte, R. Moshammer, and T. Pfeifer, Clocking Enhanced Ionization of Hydrogen Molecules with Rotational Wave Packets, Phys. Rev. Lett. **125**, 173201 (2020).

[7] L.-Y. Peng and A. F. Starace, Attosecond pulse carrier-envelope phase effects on ionized electron momentum and energy distributions, Phys. Rev. A **76**, 043401 (2007).

[8] W.-C. Jiang, W.-H. Xiong, T.-S. Zhu, L.-Y. Peng, and Q. Gong, Double ionization of He by time-delayed attosecond pulses, J. Phys. B **47**, 091001 (2014).

[9] N. F. Ramsey, A molecular beam resonance method with separated oscillating fields, Phys. Rev. **78**, 695 (1950).

[10] J. M. Ngoko Djiokap, S. X. Hu, L. B. Madsen, N. L. Manakov, A. V. Meremianin, and A. F. Starace, Electron Vortices in Photoionization by Circularly Polarized Attosecond Pulses, Phys. Rev. Lett. **115**, 113004 (2015).

[11] J. M. Ngoko Djiokap, A. V. Meremianin, N. L. Manakov, S. X. Hu, L. B. Madsen, and A. F. Starace, Multistart spiral electron vortices in ionization by circularly polarized UV pulses, Phys. Rev. A **94**, 013408 (2016).

[12] D. Pengel, S. Kerbstadt, D. Johannmeyer, L. Englert, T. Bayer, and M. Wollenhaupt, Electron Vortices in Femtosecond Multiphoton Ionization, Phys. Rev. Lett. **118**, 053003 (2017).

[13] D. Pengel, S. Kerbstadt, L. Englert, T. Bayer, and M. Wollenhaupt, Control of three-dimensional electron vortices from femtosecond multiphoton ionization, Phys. Rev. A **96**, 043426 (2017).

[14] S. Kerbstadt, K. Eickhoff, T. Bayer, and M. Wollenhaupt, Odd electron wave packets from cycloidal ultrashort laser fields, Nat. Commun. **10**, 658 (2019).

[15] S. Kerbstadt, K. Eickhoff, T. Bayer, and M. Wollenhaupt, Control of free electron wave packets by polarization-tailored ultrashort bichromatic laser fields, Adv. Phys.: X **4**, 1672583 (2019).

[16] K.-J. Yuan, S. Chelkowski, and A. D. Bandrauk, Photoelectron momentum distributions of molecules in bichromatic circularly polarized attosecond UV laser fields, Phys. Rev. A **93**, 053425 (2016).

[17] K.-J. Yuan, H. Lu, and A. D. Bandrauk, Photoionization of triatomic molecular ions $H_3^{2+}$ by intense bichromatic circularly polarized attosecond UV laser pulses, J. Phys. B **50**, 124004 (2017).

[18] J. M. Ngoko Djiokap, A. V. Meremianin, N. L. Manakov, S. X. Hu, L. B. Madsen, and A. F. Starace, Kinematical vortices in double photoionization of helium by attosecond pulses, Phys. Rev. A **96**, 013405 (2017).

[19] J. M. Ngoko Djiokap and A. F. Starace, Doubly-excited state effects on two-photon double ionization of helium by time-delayed, oppositely circularly-polarized attosecond pulses, J. Opt. **19**, 124003 (2017).

[20] Z. L. Li, Y. J. Li, and B. S. Xie, Momentum vortices on pairs production by two counter-rotating fields, Phys. Rev. D **96**, 076010 (2017).

[21] M. Li, G. Zhang, T. Zhao, X. Ding, and J. Yao, Electron vortices in photoionization by a pair of elliptically polarized attosecond pulses, Chin. Opt. Lett. **15**, 120202 (2017).

[22] J. M. Ngoko Djiokap, A. V. Meremianin, N. L. Manakov, L. B. Madsen, S. X. Hu, and A. F. Starace, Dynamical electron vortices in attosecond double photoionization of $H_2$, Phys. Rev. A **98**, 063407 (2018).

[23] M. Li, G. Zhang, X. Kong, T. Wang, X. Ding, and J. Yao, Dynamic Stark induced vortex momentum of hydrogen in circular fields, Opt. Express **26**, 878 (2018).

[24] X. Kong, G. Zhang, M. Li, T. Wang, X. Ding, and J. Yao, Odd-fold-symmetric spiral momentum distributions and their Stark distortions in hydrogen, J. Opt. Soc. Am. B **35**, 2163 (2018).

[25] D. D. A. Clarke, G. S. J. Armstrong, A. C. Brown, and H. W. van der Hart, *R*-matrix-with-time-dependence theory for ultrafast atomic processes in arbitrary light fields, Phys. Rev. A **98**, 053442 (2018).

[26] G. S. J. Armstrong, D. D. A. Clarke, J. Benda, A. C. Brown, and H. W. van der Hart, Electron correlation and short-range dynamics in attosecond angular streaking, Phys. Rev. A **101**, 041401(R) (2020).

[27] A. C. Brown, G. S. Armstrong, J. Benda, D. D. A. Clarke, J. Wragg, K. R. Hamilton, Z. Mašín, J. D. Gorfinkiel, and H. W. van der Hart, RMT: R-matrix with time-dependence. solving the semi-relativistic, time-dependent Schrödinger equation for general, multielectron atoms and molecules in intense, ultrashort, arbitrarily polarized laser pulses, Comput. Phys. Commun. **250**, 107062 (2020).

[28] X.-R. Xiao, M.-X. Wang, H. Liang, Q. Gong, and L.-Y. Peng, Proposal for Measuring Electron Displacement Induced by a Short Laser Pulse, Phys. Rev. Lett. **122**, 053201 (2019).

[29] T. Bayer, C. Philipp, K. Eickhoff, and M. Wollenhaupt, Atomic photoionization dynamics in ultrashort cycloidal laser fields, Phys. Rev. A **102**, 013104 (2020).

[30] S. Ben, S. Chen, C.-R. Bi, J. Chen, and X.-S. Liu, Investigation of electron vortices in time-delayed circularly polarized laser pulses with a semiclassical perspective, Opt. Express **28**, 29442 (2020).

[31] J. Sörngård, J. M. Dahlström, and E. Lindroth, Study of the possibilities with combinations of circularly and linearly polarized light for attosecond delay investigations, J. Phys. B **53**, 134003 (2020).

[32] R. Kienberger, E. Goulielmakis, M. Uiberacker, A. Baltuska, V. Yakovlev, F. Bammer, A. Scrinzi, T. Westerwalbesloh, U. Kleineberg, U. Heinzmann, M. Drescher, and F. Krausz, Atomic transient recorder, Nature **427**, 817 (2004).

[33] B. Bergues, D. E. Rivas, M. Weidman, A. A. Muschet, W. Helml, A. Guggenmos, V. Pervak, U. Kleineberg, G. Marcus, R. Kienberger, D. Charalambidis, P. Tzallas, H. Schröder, F. Krausz, and L. Veisz, Tabletop nonlinear optics in the 100-eV spectral region, Optica **5**, 237 (2018).

[34] J. Duris, S. Li, T. Driver, E. G. Champenois, J. P. MacArthur, A. A. Lutman, Z. Zhang, P. Rosenberger, J. W. Aldrich, R. Coffee, G. Coslovich, F.-J. Decker, J. M. Glownia, G. Hartmann, W. Helml, A. Kamalov, J. Knurr, J. Krzywinski, M.-F. Lin, J. P. Marangos, M. Nantel, A. Natan, J. T. O'Neal, N. Shivaram, P. Walter, A. L. Wang, J. J. Welch, T. J. A. Wolf, J. Z. Xu, M. F. Kling, P. H. Bucksbaum, A. Zholents, Z. Huang, J. P. Cryan, and A. Marinelli, Tunable isolated attosecond X-ray pulses with gigawatt peak power from a free-electron laser, Nat. Photonics **14**, 30 (2019).

[35] P.-C. Huang, C. Hernández-García, J.-T. Huang, P.-Y. Huang, C.-H. Lu, L. Rego, D. D. Hickstein, J. L. Ellis, A. Jaron-Becker, A. Becker, S.-D. Yang, C. G. Durfee, L. Plaja, H. C. Kapteyn, M. M. Murnane, A. H. Kung, and M.-C. Chen, Polarization control of isolated high-harmonic pulses, Nat. Photonics **12**, 349 (2018).

[36] A. S. Davydov, *Quantum Mechanics*, 2nd ed. (Pergamon Press, Oxford, 1976).

[37] E. A. Pronin, A. F. Starace, M. V. Frolov, and N. L. Manakov, Perturbation theory analysis of attosecond photoionization, Phys. Rev. A **80**, 063403 (2009).

[38] N. L. Manakov, S. I. Marmo, and A. V. Meremianin, A new technique in the theory of angular distributions in atomic processes: The angular distribution of photoelectrons in single and double photoionization, J. Phys. B **29**, 2711 (1996).

[39] S. D. Oh and R. H. Pratt, Nonvanishing of allowed Coulomb dipole matrix elements, Phys. Rev. A **34**, 2486 (1986).

[40] N. L. Manakov and A. G. Fainshtein, Quasistationary quasi-energy states and convergence of perturbation series in a monochromatic field, Theor. Math. Phys. **48**, 815 (1981).

[41] J. M. Ngoko Djiokap, N. L. Manakov, A. V. Meremianin, S. X. Hu, L. B. Madsen, and A. F. Starace, Nonlinear Dichroism in Back-to-Back Double Ionization of He by an Intense Elliptically Polarized Few-Cycle Extreme Ultraviolet Pulse, Phys. Rev. Lett. **113**, 223002 (2014).

[42] M. S. Pindzola and F. Robicheaux, Total ionization cross section for electron-hydrogen scattering using a time-dependent close-coupling method, Phys. Rev. A **54**, 2142 (1996).

[43] M. S. Pindzola and F. Robicheaux, Time-dependent close-coupling calculations of correlated photoionization processes in helium, Phys. Rev. A **57**, 318 (1998).

[44] C. W. McCurdy, M. Baertschy, and T. N. Rescigno, Solving the three-body Coulomb breakup problem using exterior complex scaling, J. Phys. B **37**, R137 (2004).

[45] S. X. Hu, Optimizing the FEDVR-TDCC code for exploring the quantum dynamics of two-electron systems in intense laser pulses, Phys. Rev. E **81**, 056705 (2010).

[46] H. G. Muller, An efficient propagation scheme for the time-dependent Schrödinger equation in the velocity gauge, Laser Phys. **9**, 138 (1999).

[47] T. K. Kjeldsen, L. A. A. Nikolopoulos, and L. B. Madsen, Solving the $m$-mixing problem for the three-dimensional time-dependent Schrödinger equation by rotations: Application to strong-field ionization of $H_2^+$, Phys. Rev. A **75**, 063427 (2007).

[48] J. M. Ngoko Djiokap, S. X. Hu, W.-C. Jiang, L.-Y. Peng, and A. F. Starace, Enhanced asymmetry in few-cycle attosecond pulse ionization of He in the vicinity of autoionizing resonances, New J. Phys. **14**, 095010 (2012).